Supplementary Information for:

ESR-thermochronometry of the Hida range of the Japanese Alps: Validation and future potential

Georgina E. King[1], Sumiko Tsukamoto[2], Frédéric Herman[1], Rabiul H. Biswas[1], Shigeru Sueoka[3] and Takahiro Tagami[4]

[1]Institute of Earth Surface Dynamics, University of Lausanne, Lausanne, Switzerland
[2]Leibniz Institute for Applied Geophysics, Hannover, Germany
[3]Tono Geoscience Center, Japan Atomic Energy Agency, Toki, Japan
[4]Division of Earth and Planetary Sciences, Kyoto University, Kyoto, Japan

Correspondence to: Georgina E. King (georgina.king@unil.ch)

Contents:

S1. Model Selection

S1.1 Model selection for ESR data

Toyoda and Ikeya (1991) and Ikeya (1993) found that the thermal decay of the Al and Ti centres could be well described using a second order kinetic model. We tested fitting the ESR isothermal decay data using a first order kinetic model and also using a general order approach following Guralnik et al. (2015).

General order kinetic model

A general order kinetic model describing signal accumulation in a saturating system corresponds to:

$$\frac{d\tilde{n}}{dt} = \widetilde{D}(1-\tilde{n}) - (\tilde{n})^b s \exp\left(-\frac{E_t}{k_b T}\right) \quad \text{(S1)}$$

where $\tilde{n}$ is the fraction of saturation (n/N), $\widetilde{D}$ is defined as $\dot{D}/D_0$ where $\dot{D}$ is the environmental dose rate (Gy/ka) and D_0 is the characteristic dose of saturation (Gy), b is the kinetic order, E_t is the trap depth (eV), k_b is Boltzmann's constant (eV/K) and T is temperature (K).

During isothermal holding experiments, no signal accumulation occurs:

$$\frac{d\tilde{n}}{dt} = -(\tilde{n})^b s \exp\left(-\frac{E_t}{k_b T}\right) \quad \text{(S2)}$$

and the temperature is constant, so one can integrate such that:

$$\tilde{n} = \left((\tilde{n})_0^{1-b} - (1-b)\, s \exp\left(-\frac{E_t}{k_b T}\right)\right)^{\frac{1}{1-b}} \quad \text{(S3)}$$

where $(\tilde{n})_0$ is the fraction of saturation at the beginning of the isothermal holding experiment. Guralnik et al. (2015a; b) used this model to successfully fit feldspar luminescence isothermal decay data, under the assumption that the initial trapped charge concentration, $(\tilde{n})_0 = 1$. Lambert et al. (In Revision) investigated this assumption, by instead using the true fraction of saturation as the initial condition when fitting their feldspar luminescence isothermal decay data; we follow the approach of Lambert et al. (In Revision). Whilst the Ti centre experiences signal saturation and Eq. (S3) can be fitted to the isothermal decay data both with the true fraction of saturation or assuming $(\tilde{n})_0 = 1$, the Al centre of the KRG samples does not exhibit saturation and a modified equation must be used. If we convert these equations in terms of dose, D (Gy), which is related to signal intensity, I, ESR growth can be expressed as:

$$\frac{dD}{dt} = \dot{D} \quad \text{(S4)}$$

and thermal decay is given by:

$$\frac{dD}{dt} = -D^b s \exp(-\frac{E_t}{k_b T}) \quad \text{(S5)}$$

and in turn thermal holding data can be fitted using:

$$D = (D_{t=0}^{1-b} - (1-b)\, s \exp\left(-\frac{E_t}{T \cdot k_B}\right))^{\frac{1}{1-b}} \quad \text{(S6)}$$

where $D_{t=0}$ is the initial dose given to the samples. Finally, because the data are normalized relative to the first measurement, this becomes:

$$D/D_{t=0} = \frac{D_{t=0}^{1-b} - (1-b)\, s \exp\left(-\frac{E_t}{T \cdot k_B}\right))^{\frac{1}{1-b}}}{D_{t=0}} \quad \text{(S7)}$$

Fitting of experimental data

The isothermal decay data for both the Al and Ti centres were initially fitted using a first order kinetic model, however this was unable to describe the data (Fig. S1a,b). The data were then fitted using Eq. (S3) assuming an initial condition of $(\tilde{n})_0$=1. These fits resulted in kinetic orders of between 4 and 6 (Fig. S.1c,d, Table S1.1). Toyoda and Ikeya (1991) found that the thermal decay of the Al and Ti centres could be described by second order kinetics, however it was not possible to fit the samples in this study when the kinetic order was forced to ≤2. Where the initial condition of the isothermal decay experiment was included for fitting the data (Eq. (S3) for the Ti centre, or Eq. (S7) for the Al centre), very low values of *s* were obtained for the Al-centre, caused by a trade-off with the initial condition (Table S1.1). This effect is relatively minor for the Ti-centre for measurements in response to 4.3 kGy, because the initial condition of ~0.8 is close to 1 (Table S1.1). General order kinetics predicts that the rate of charge detrapping is dependent on the trapped charge concentration (Fig. S1.2a,b), we measured the isothermal decay of sample KRG16-104 following two different doses of 4.30 kGy and 2.15 kGy to confirm whether the ESR response is dose dependent (Fig. S1.2c-f). However, whereas dose dependent effects are predicted (Fig. S1.2a,b) no clear dose dependency is apparent in the data (Fig. S1.2c-f), although a greater difference in the Al-centre data is recorded than the Ti-centre data. This may indicate that general order kinetics is not appropriate for describing the isothermal decay of the Al or Ti

centre, however this result should be regarded with caution because inter-aliquot variability and slight variations in experimental conditions (e.g. aliquot positioning between measurements) could also induce differences in the data.

S1.2 Model selection for luminescence data

A range of models have been proposed that describe charge trapping and detrapping processes in feldspar minerals (cf. Gurlanik et al., 2015b). Guralnik et al. (2015a) validated a general order kinetic model (GOK) for luminescence dose response and thermal decay against a dataset of feldspar samples with known thermal history from the KTB borehole in Germany. More recently Lambert et al. (In Review) tested two further models for feldspar thermal decay, based on a distribution of thermal trap lifetimes, against the same dataset, validating both approaches. These latter models are the band-tail states model (BTS; Li and Li, 2013) and a Gaussian trap distribution model (GAU; Lambert et al., In Review). Lambert et al. (In Review) used a GOK fit for luminescence dose response in their validation study, however using a single saturating exponential fit (1EXP) also results in trapped-charge concentration estimations, commensurate with the independent temperature control of those samples. However, despite these validation studies, the luminescence behaviour of different feldspar minerals has been observed to vary (Lambert et al., In Revision; Riedesel et al., 2018); consequently, it is necessary to evaluate which model is appropriate for the feldspar samples under investigation in the present study.

Electron trapping: luminescence dose response

The luminescence dose response of feldspar is relatively unstudied with the exception of two investigations on the natural dose response of feldspar samples extracted from the Luochoan loess plateau (Li and Li, 2011; Li et al., 2018). These studies both found that the natural dose response of feldspar could be well described with 1EXP, although it should be recognized that it remains unknown whether the properties of feldspar minerals extracted from loess differ to those of feldspar extracted from bedrock. King et al. (2018) have shown that using a GOK, rather than 1EXP model for luminescence dose response can result in underestimation of the luminescence trapped charge concentration. For this reason, in this study, although feldspar dose response would be better described using a GOK model, we instead use 1EXP to fit all of the feldspar dose response data (see luminescence data fits in part S2 of the Supplementary Materials).

Electron detrapping: luminescence thermal decay

Lambert et al. (In Revision) investigated which model could best describe the thermal decay of their feldspar samples from the Mont Blanc massif. They found that the mathematical assumptions that underpin the GOK model were not appropriate for their samples (see also discussion in part S1.1). Furthermore, the BTS model was unable to fully describe their isothermal decay data, especially for measurements made following high temperature (>200 °C) isothermal holding for long durations (>2000 s). On this basis, Lambert et al. (In Revision) selected the GAU model as most appropriate for their samples, due to its improved ability to fit their experimental data, and validation of this model against feldspar data from the KTB borehole (Lambert et al., In Review; Guralnik et al., 2015a).

In the present study, in addition to the feldspar OSL data, the ESR data provide relative constraint on feldspar luminescence thermal stability. This is because for a single sample, both the ESR and OSL systems have experienced exactly the same thermal history, and thus a system with an older age should be more thermally stable. As shown in Tables 1 and 2 of the main text, the OSL ages of samples KRG16-104 and KRG16-06 are slightly younger in comparison to the ESR ages for these samples, although the ages are similar. This indicates that the thermal stability of the luminescence centres should be slightly lower than the ESR centres for these samples. In contrast, for sample KRG16-101 the OSL ages are older than the ESR ages, suggesting that the OSL centres should exhibit higher thermal stability. As the OSL ages of sample KRG16-05 are saturated no contrast can be made with the ESR ages for this sample.

The isothermal decay data measured for the different feldspar signals can be described well using either the BTS or GAU models (Figure S1.3), although as reported by Lambert et al. (In Revision), some deviation is recorded between the model prediction of the BTS model, and the experimental data (Fig. S1.3a). In order to visualize the thermal stability of the different models, isothermal decay can be modelled for a specific temperature over geological time. Whilst in luminescence dating it is standard to consider trap thermal stability at 20 °C (i.e. for sediment dating, Aitken, 1985) we consider it here at 60 °C which is nearer to the closure temperature constrained for the luminescence system (sample and signal dependent, Fig. S1.4; cf. Guralnik et al., 2013; King et al., 2016). For all samples, the BTS model predicts lower thermal stability for the OSL signals, relative to the ESR signals. In contrast when the GAU model is used, both systems exhibit similar thermal stability for all samples. If the ESR and OSL ages are taken as robust control on the relative thermal stability of the ESR and OSL systems, and assuming that the uncertainties calculated for the ESR and OSL ages are not underestimated, it seems that the GAU model may slightly overestimate the thermal stability of these feldspar samples. Significantly, for sample KRG16-101, neither model results in the OSL data having higher thermal stability than the ESR data, which is predicted from the difference in ages between the two dating approaches. This discrepancy likely reflects uncertainties in the measurements made, possibly in the ESR data, which cannot presently be measured within an automated system. This discrepancy may alternatively reflect the challenges of constraining thermal kinetic parameters within the laboratory (e.g. Schmidt et al., 2018) and/or the difficulties associated with measuring anomalous fading.

In order to evaluate the effect of using the different thermal kinetic models on the cooling histories obtained, the luminescence data were inverted using both the GAU kinetic parameters and model and then using the BTS kinetic parameters and model, results are shown in Fig. S1.5. The cooling histories determined using the two models are similar, although the GAU model yields more rapid cooling. This is because this model predicts higher thermal stability for the IRSL signals, as revealed in Fig. S1.4., which is inconsistent with the ESR data. We therefore opt to use the BTS model to describe feldspar luminescence thermal decay in this study.

Table S1.1: ESR centre thermal kinetic parameters calculated using general order kinetics. All uncertainties are listed at 1σ. Measurements were made in response to a 4.30 kGy dose except for the second measurement of KRG16-104 which was made in response to a 2.15 kGy dose.

Al	Et	$\log_{10}(s)$	b
Initial condition = 1			
KRG16-05	1.25 ± 0.08	11.27 ± 0.96	4.22 ± 0.31
KRG16-06	1.61 ± 0.10	16.17 ± 1.25	4.28 ± 0.31
KRG16-101	1.55 ± 0.16	14.85 ± 1.96	4.33 ± 0.36
KRG16-104	1.16 ± 0.17	9.87 ± 2.01	4.25 ± 0.53
KRG16-104 (2)	1.50 ± 0.20	14.09 ± 2.32	4.27 ± 0.60
Initial condition = ITL dose			
KRG16-05	1.25 ± 0.08	-0.43 ± 1.14	4.22 ± 0.31
KRG16-06	1.61 ± 0.10	4.27 ± 0.98	4.28 ± 0.31
KRG16-101	1.55 ± 0.16	2.76 ± 1.94	4.33 ± 0.36
KRG16-104	1.16 ± 0.17	-1.92 ± 1.88	4.25 ± 0.53
KRG16-104 (2)	1.50 ± 0.19	3.29 ± 1.99	4.27 ± 0.55
Ti			
Initial condition = 1			
KRG16-05	1.38 ± 0.10	12.81 ± 1.13	4.70 ± 0.37
KRG16-06	1.64 ± 0.10	16.35 ± 1.18	5.05 ± 0.34
KRG16-101	2.05 ± 0.16	20.70 ± 1.93	6.00 ± 0.35
KRG16-104	1.31 ± 0.16	11.25 ± 1.89	4.33 ± 0.50
KRG16-104 (2)	1.40 ± 0.12	12.32 ± 1.40	5.21 ± 0.44
Initial condition = fraction of saturation calculated for ITL dose			
KRG16-05	1.38 ± 0.10	12.94 ± 1.14	4.70 ± 0.37
KRG16-06	1.64 ± 0.10	16.68 ± 1.20	5.05 ± 0.34
KRG16-101	2.05 ± 0.16	21.21 ± 1.94	6.00 ± 0.35
KRG16-104	1.31 ± 0.16	11.70 ± 1.91	4.33 ± 0.50
KRG16-104 (2)	1.40 ± 0.12	13.66 ± 1.45	5.20 ± 0.44

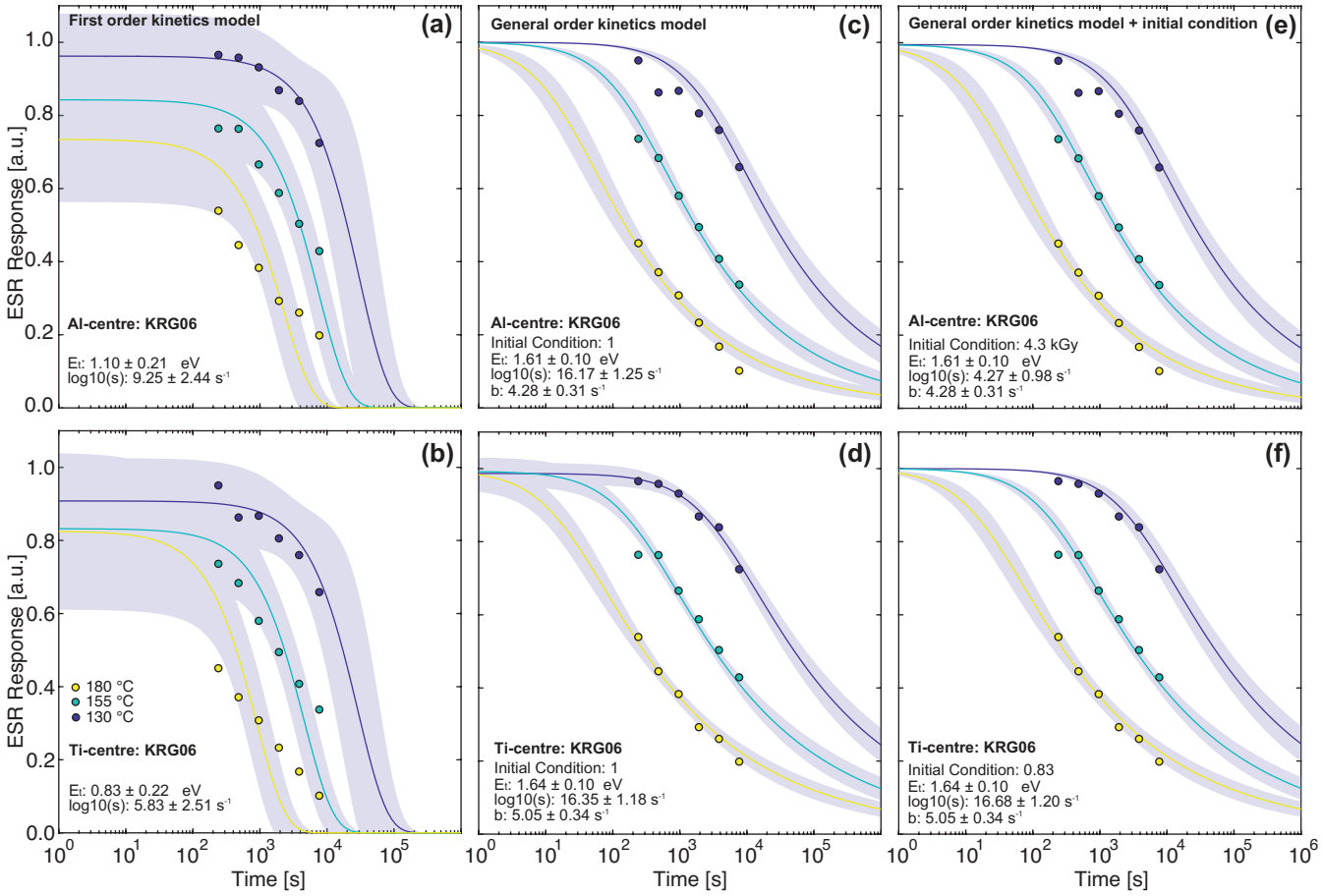

Figure S1.1: Isothermal holding data for the Al (a,c,e) and Ti (b,d,f) centres of sample KRG16-06 fitted with first-order kinetics (a,b) and general-order kinetics using an initial condition of $(\tilde{n})_0 = 1$ (c,d) and with the true initial condition (e,f) as discussed in the main text.

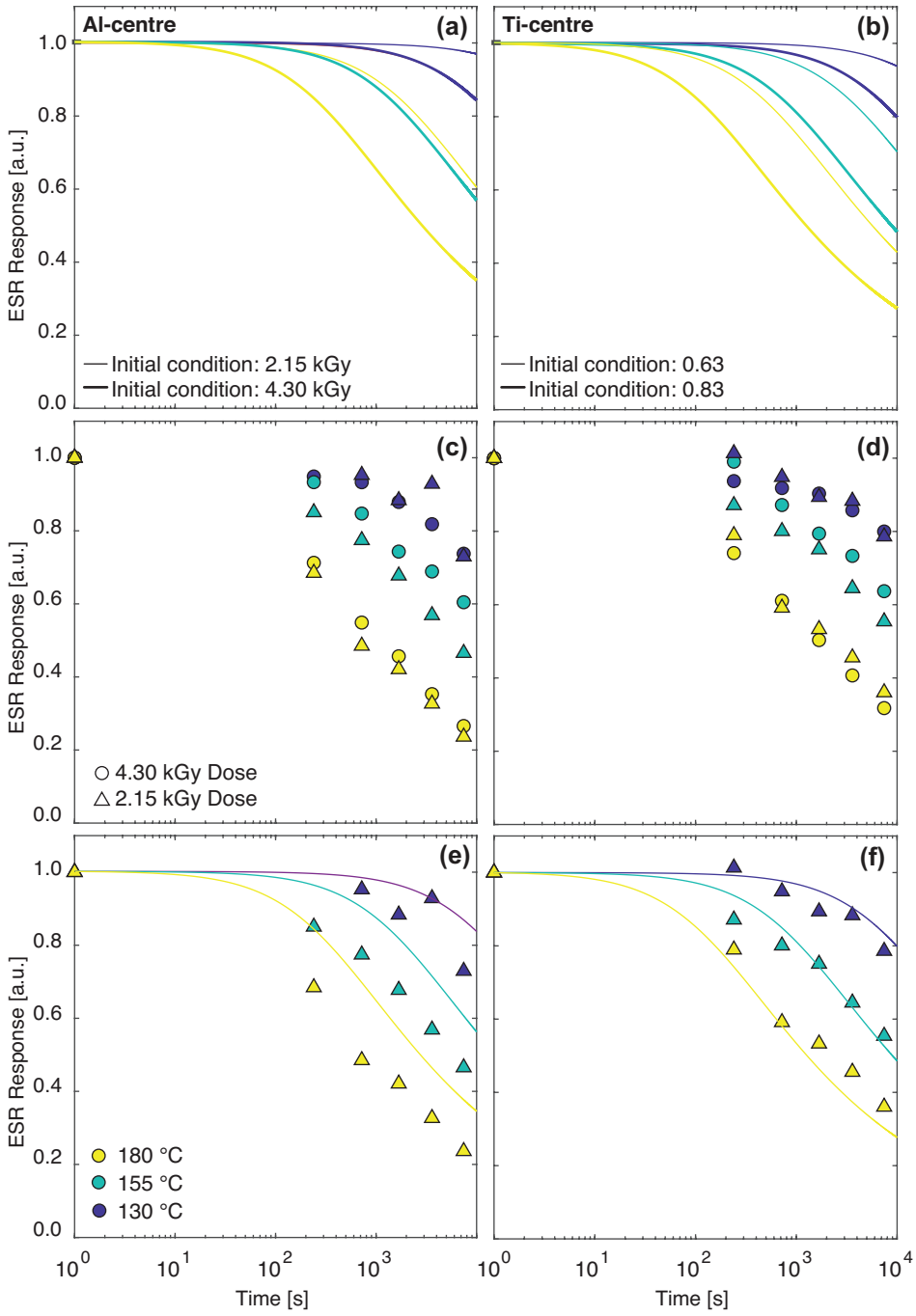

Figure S1.2: Dose dependency of signal thermal decay predicted for the Al and Ti centres using a general order kinetic model. (a,b) Prediction of isothermal decay for different initial conditions, based on parameters measured for KRG16-104 following a 4.30 kGy dose. (c,d) Measured ESR signal intensities for isothermal decay following a 4.30 kGy and 2.15 kGy dose. (e,f) Comparison of data measured following a 2.15 kGy dose with thermal decay predicted from parameters fitted for a 4.30 kGy dose.

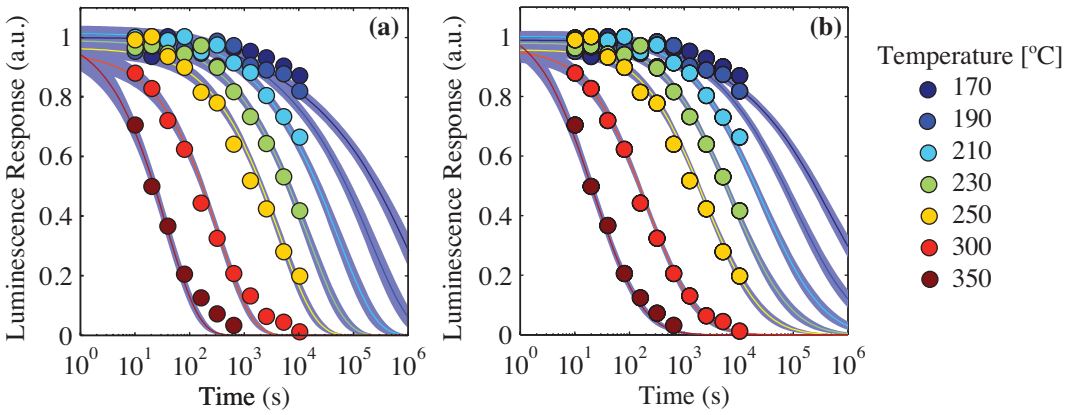

Figure S1.3: Isothermal decay data for the $IRSL_{100}$ signal of sample KRG16-06 fitted with (a) the BTS model (Li and Li, 2013) and (b) the GAU model (Lambert et al., In Review). Note the slight deviation of the data from the model fits at the highest temperatures in (a).

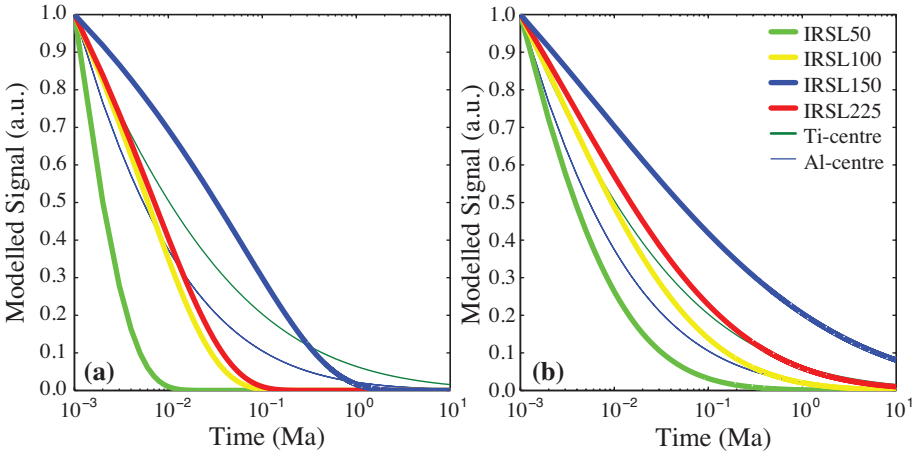

Figure S1.4: Modelled isothermal decay for the different IRSL signals of sample KRG16-06 using the kinetic parameters determined with (a) the BTS model and (b) the GAU model. The isothermal decay of the Al and Ti centres are also shown for comparative purposes. Modelling is done assuming isothermal conditions of 60 °C.

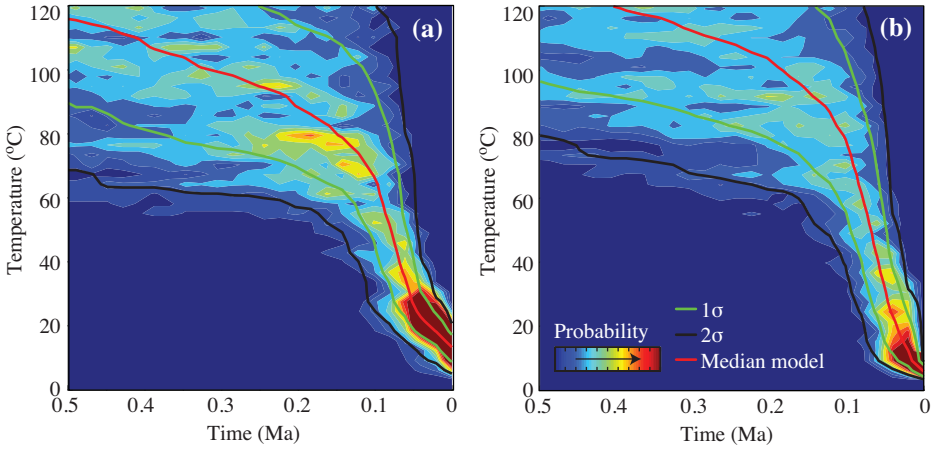

Figure S1.5: Inversion of sample KRG16-06 using thermal kinetic parameters determined from (a) the BTS model and (b) the GAU model. Inversions were done using Eq. (5) and Eq. (1) in the main text respectively and were run from 200 °C to 15 ± 5 °C for 2 Ma; only the last 0.5 Myr are shown.

S2: Electron Spin Resonance Data Fitting

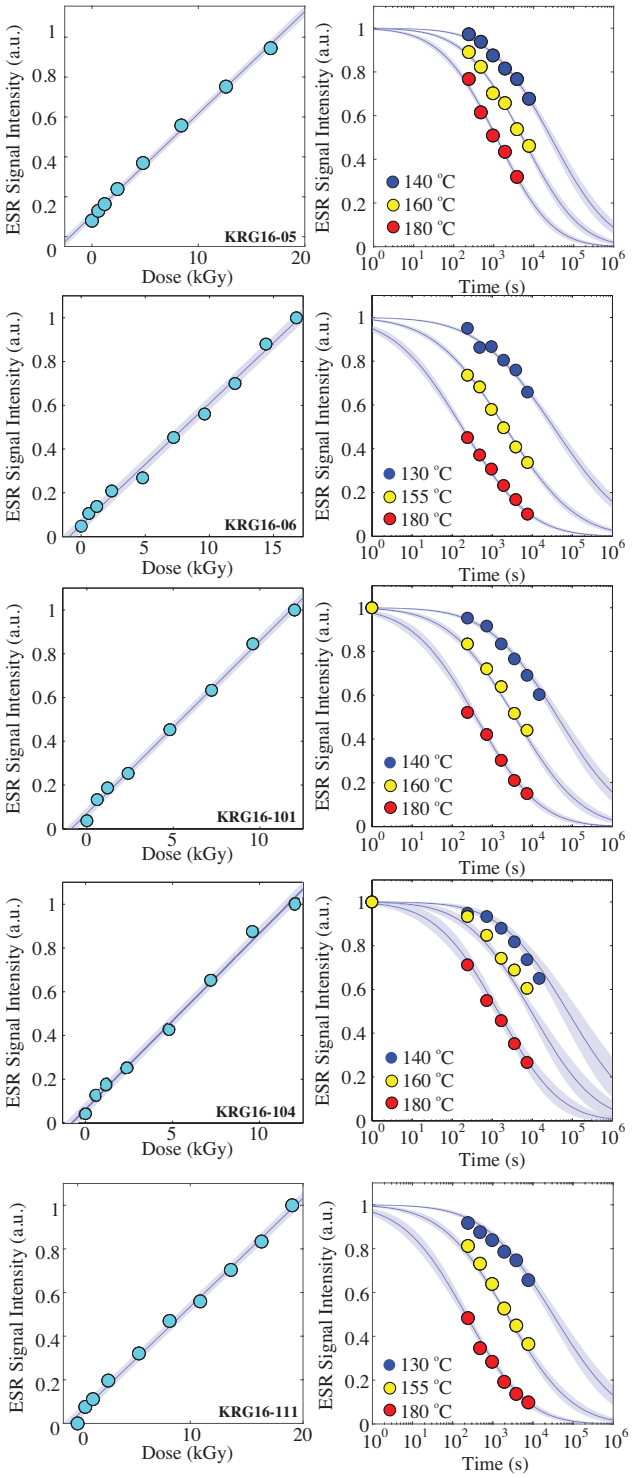

Figure S2.1: Fitting of the ESR Al-centre. Panels on the left show characterisation of natural dose response whereas panels on the right show isothermal decay data fitted with the GAU model.

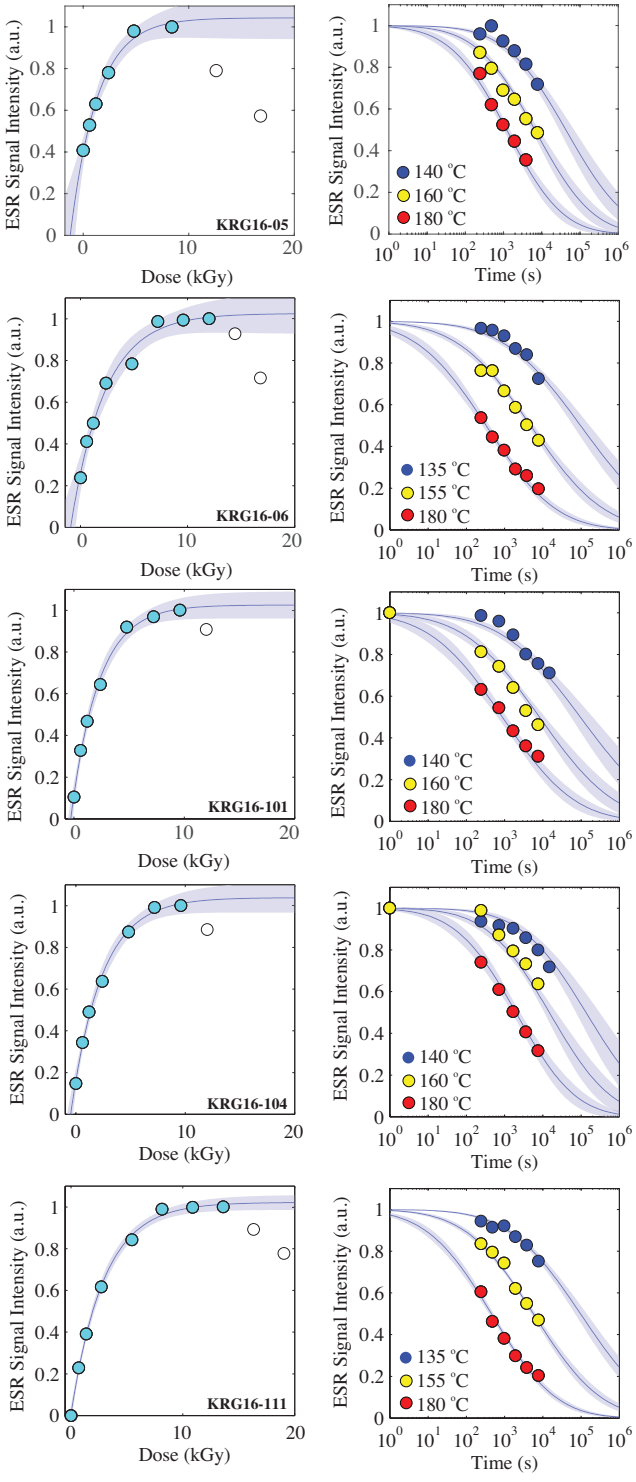

Figure S2.2: Fitting of the ESR Ti-centre. Panels on the left show characterisation of natural dose response whereas panels on the right show isothermal decay data fitted with the GAU model. White data points are excluded from the data fitting (see main text for further details).

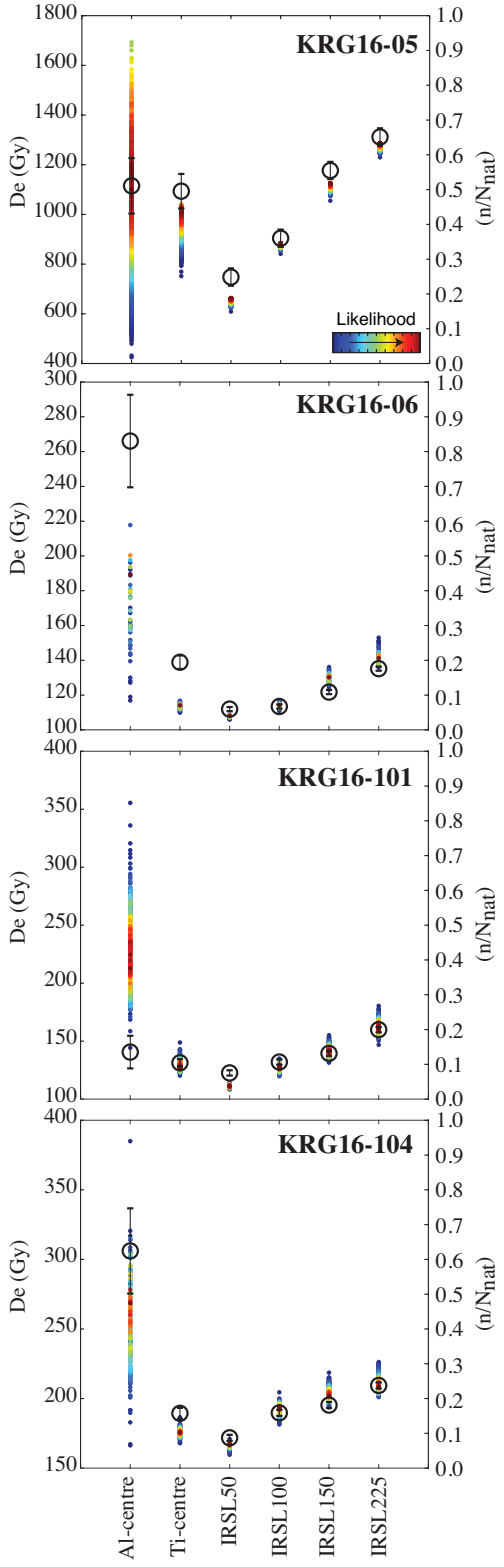

Figure S2.3: Model residuals following inversion of the Al- and Ti-centres together with the OSL data for samples KRG16-05, KRG16-06, KRG16-101 and KRG16-104. The Al-centre data alone are plotted relative to the primary y-axis, whilst the remainder of the data are plotted relative to the secondary y-axis. The inversion results are shown in Fig. 4 of the main text. For some samples the misfit between measured values (open circles) and modelled values (coloured circles) is high, possibly reflecting uncertainties in the derivation of experimental parameters e.g. for the Al- and Ti-centres of KRG16-06 and the Al-centre of KRG16-101.

S3: Luminescence Data Fitting

S3.1 Luminescence measurement acceptance criteria

All luminescence signals fulfilled the following acceptance criteria of (1) signal >3σ above background, (2) recycling ratio within 10% of unity, (3) recuperation <5% of the natural luminescence signal, (4) maximum test dose uncertainty 10%. Luminescence signals were integrated across the first 2.4 s of stimulation, whilst background signals were integrated across the final 20 s of stimulation.

S3.2 Confirmation of feldspar luminescence data thermal signal

In order to confirm whether the feldspar samples contain a thermal signal, they were screened using the Huntley (2006) model following Kars et al. (2008) (cf. Gurlanik et al., 2015; Valla et al., 2016, Fig. S3.1). All four signals for sample KRG16-05 plot within 15% of $(n/N)_{ss}$ and therefore do not contain any information on rock cooling histories; rather the luminescence signals represent an equilibrium between rates of electron trapping and athermal electron detrapping. The $IRSL_{50}$ signals of samples KRG16-06 and KRG16-101, which are most affected by anomalous fading are also saturated. In contrast, the high temperature signals from these samples, and all signals from sample KRG16-104 and the naturally zero age samples KRG16-111 and KRG16-112 are not in field saturation.

S3.3 Feldspar luminescence dose recovery

In order to confirm that the selected measurement protocol is appropriate, a dose recovery experiment was performed on samples KRG16-05, KRG16-06 and KRG16-101. Six new aliquots were prepared and then bleached using natural sunlight in Bern for between 4 and 6 hours. A dose similar to the natural (faded) measured equivalent dose for the $IRSL_{50}$ signal was then administered to three of the aliquots, whilst the other three were measured to constrain any unbleached residual signal. Residual subtracted recovered doses are summarized in Figure S3.2.

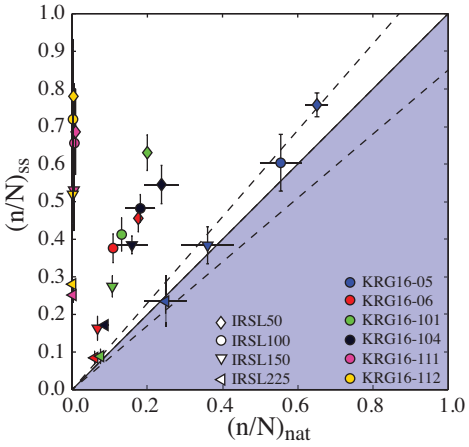

Figure S3.1: Screening of feldspar luminescence signals for field saturation. The dashed lines are 15% from $(n/N)_{ss}$ and indicate the limit of detection for the luminescence thermochronometry method (cf. Guralnik et al., 2015a).

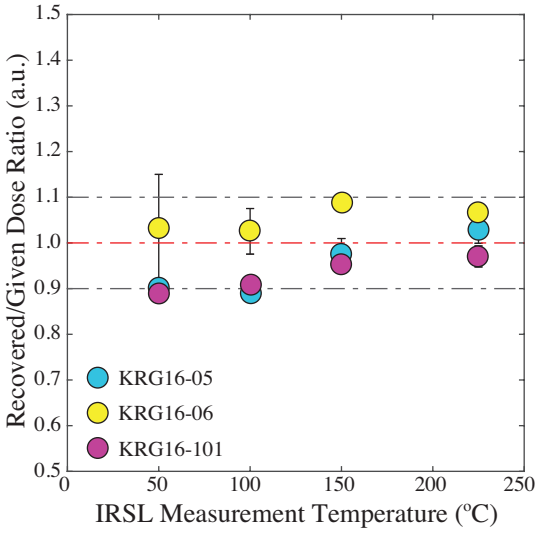

Figure S3.2: Residual subtracted dose recovery ratios for samples KRG16-05, KRG16-06 and KRG16-101.

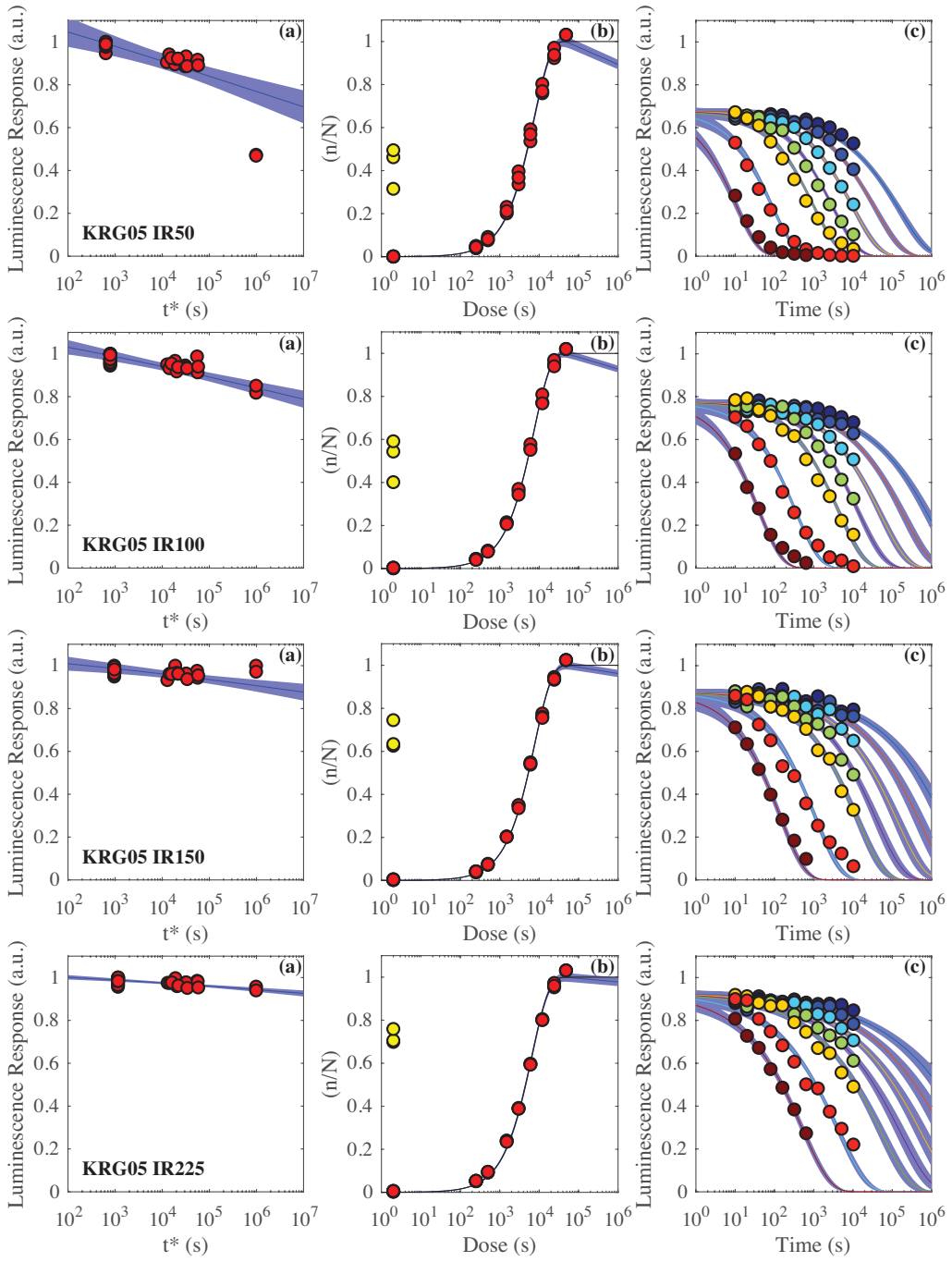

Figures S3.3: Fitting of luminescence thermochronometry data for sample KRG16-05. (a) Anomalous fading data. (b) Luminescence dose response data fitted with a single saturating exponential function. Yellow dots are the natural luminescence signal whereas red dots are the regenerative doses. (c) Luminescence isothermal decay data fitted with the BTS model.

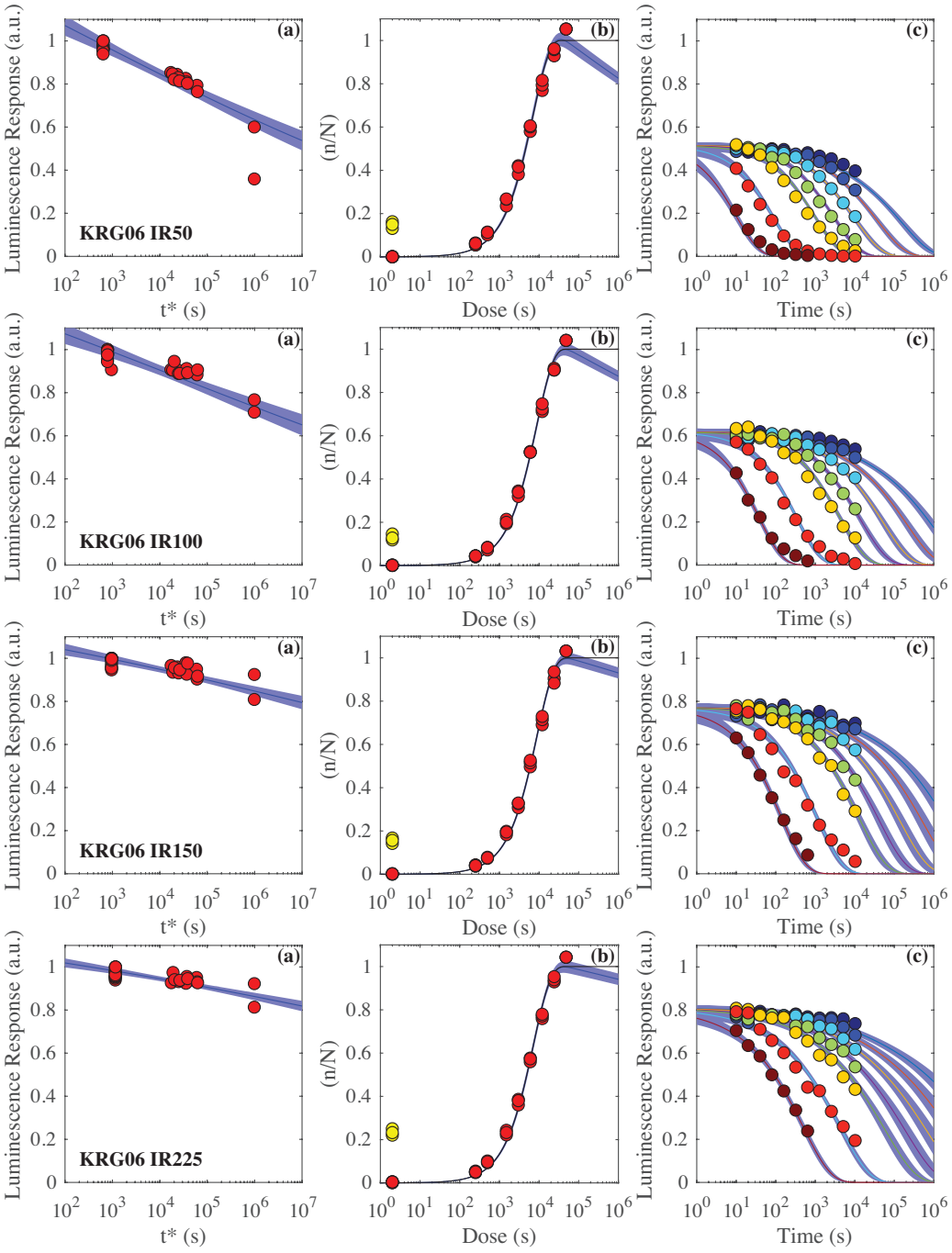

Figures S3.4: Fitting of luminescence thermochronometry data for sample KRG16-06. (a) Anomalous fading data. (b) Luminescence dose response data fitted with a single saturating exponential function. Yellow dots are the natural luminescence signal whereas red dots are the regenerative doses. (c) Luminescence isothermal decay data fitted with the BTS model.

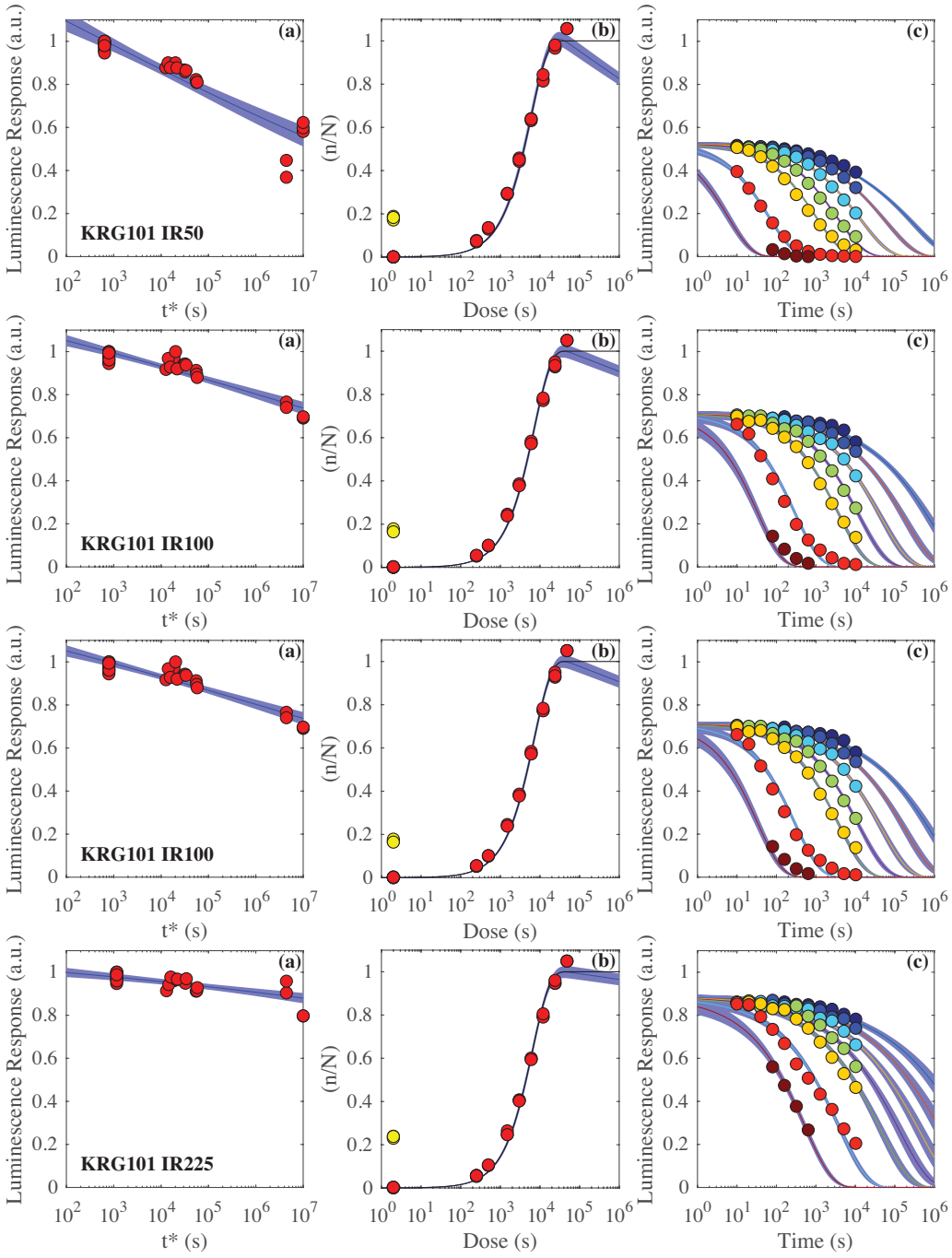

Figures S3.5: Fitting of luminescence thermochronometry data for sample KRG16-101. (a) Anomalous fading data. (b) Luminescence dose response data fitted with a single saturating exponential function. Yellow dots are the natural luminescence signal whereas red dots are the regenerative doses. (c) Luminescence isothermal decay data fitted with the BTS model.

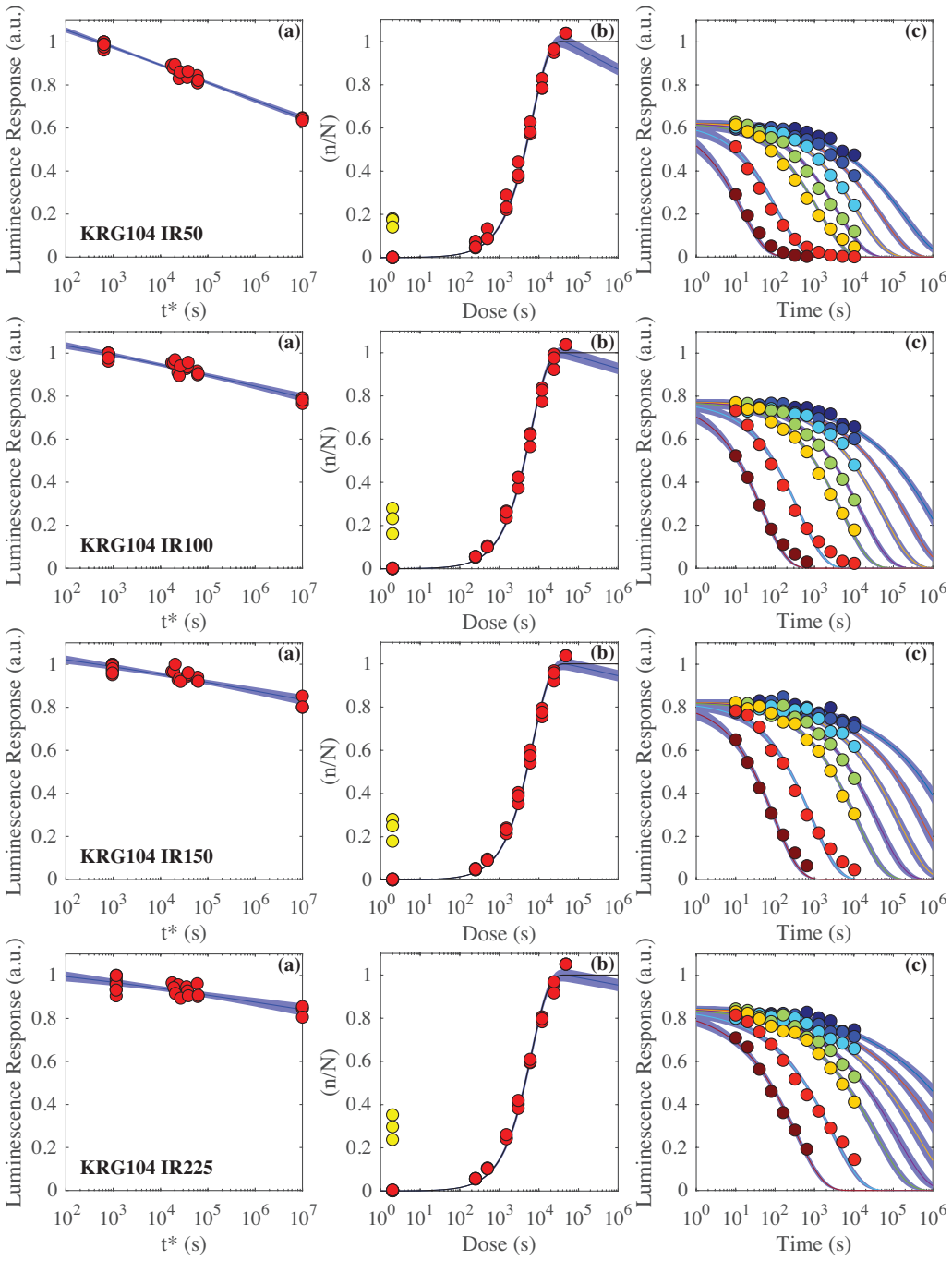

Figures S3.6: Fitting of luminescence thermochronometry data for sample KRG16-104. (a) Anomalous fading data. (b) Luminescence dose response data fitted with a single saturating exponential function. Yellow dots are the natural luminescence signal whereas red dots are the regenerative doses. (c) Luminescence isothermal decay data fitted with the BTS model.

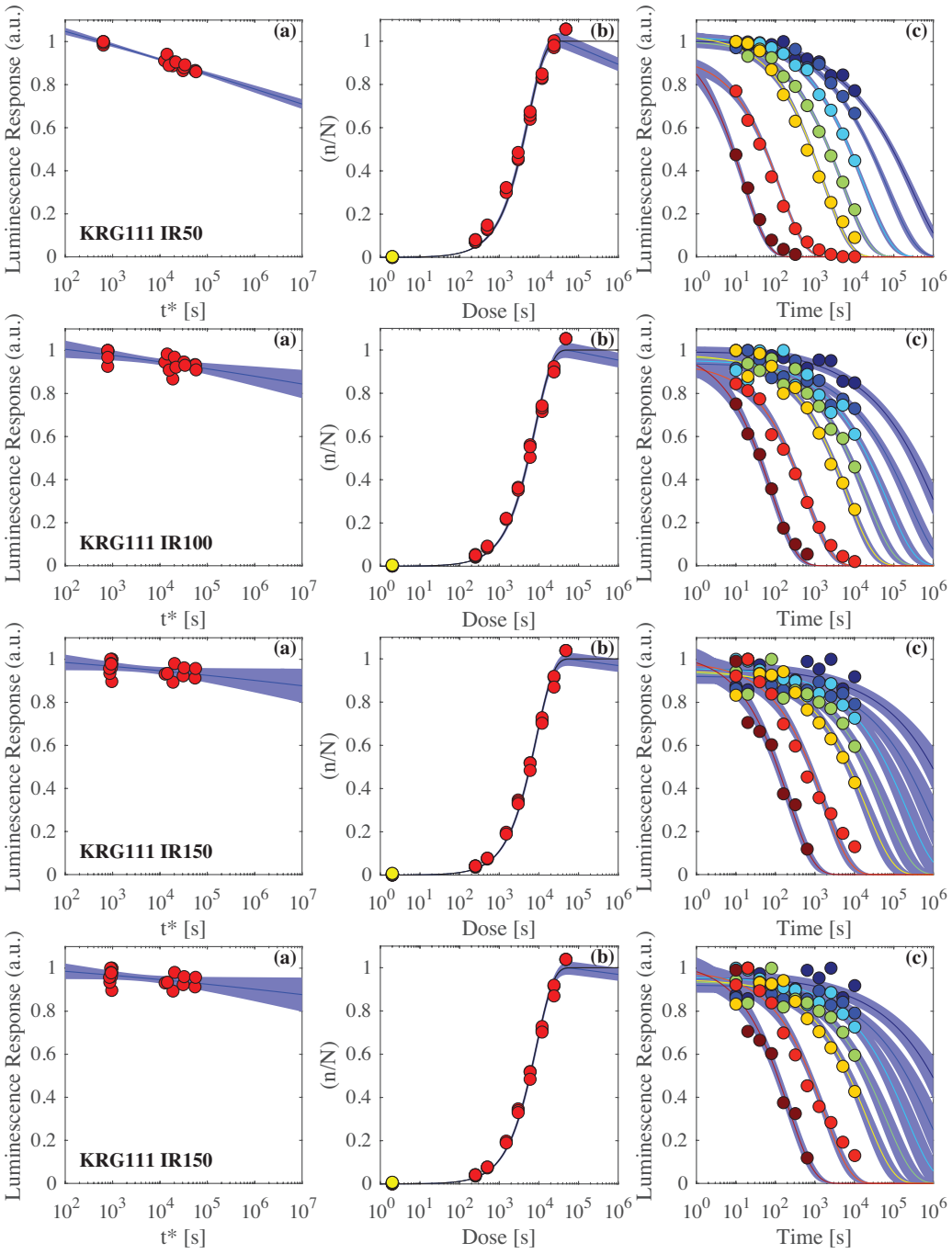

Figures S3.7: Fitting of luminescence thermochronometry data for sample KRG16-111. (a) Anomalous fading data. (b) Luminescence dose response data fitted with a single saturating exponential function. Yellow dots are the natural luminescence signal whereas red dots are the regenerative doses. (c) Luminescence isothermal decay data fitted with the BTS model.

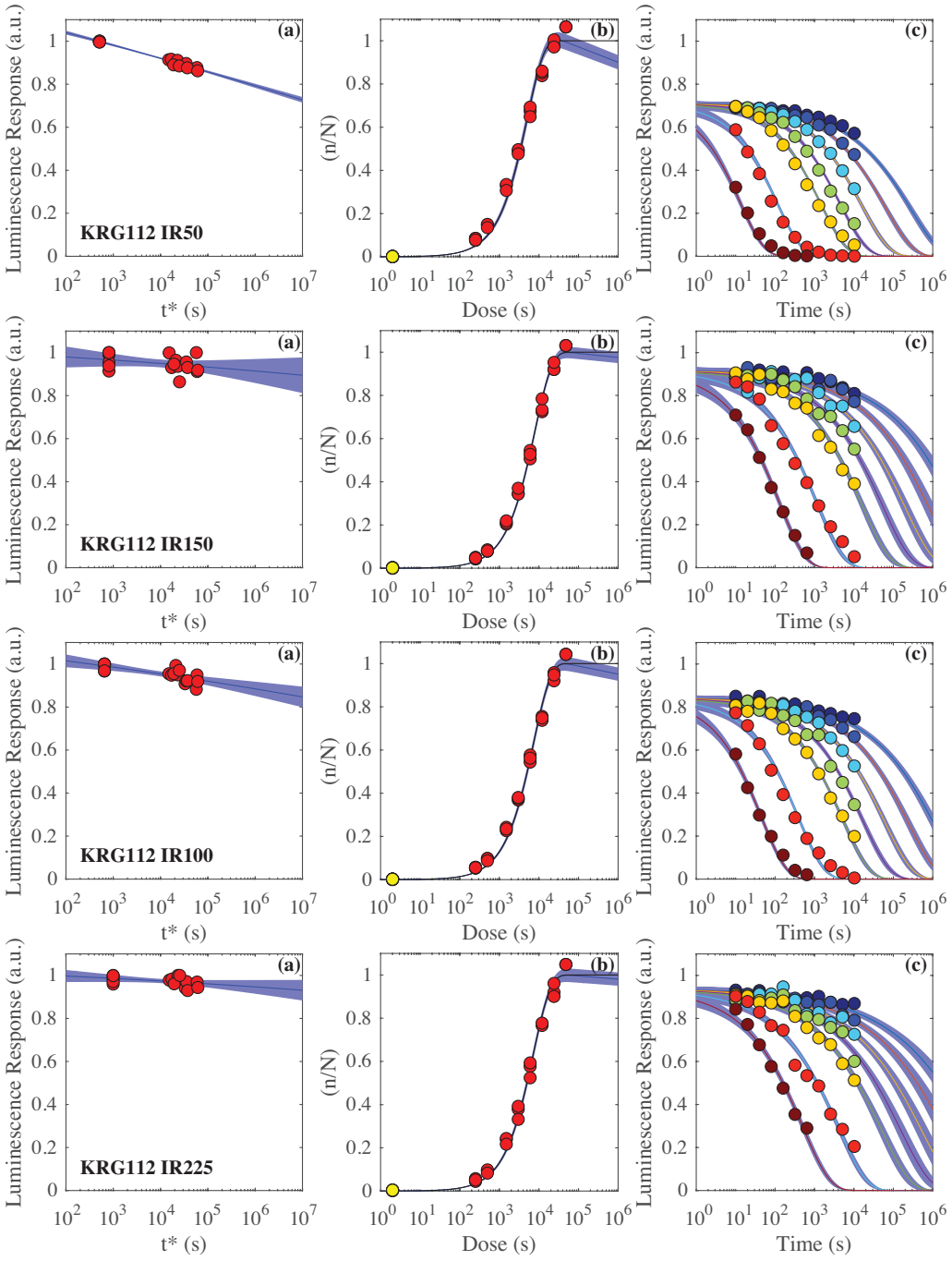

Figures S3.8: Fitting of luminescence thermochronometry data for sample KRG16-112. (a) Anomalous fading data. (b) Luminescence dose response data fitted with a single saturating exponential function. Yellow dots are the natural luminescence signal whereas red dots are the regenerative doses. (c) Luminescence isothermal decay data fitted with the BTS model.

5

S.4 Sample Locations

Table S4.1: Sample locations.

Sample Name	Elevation (m)	Latitude	Longitude
KRG16-05	2,134	137.6473	36.6349
KRG16-06	1,884	137.6510	36.6402
KRG16-101	1,605	137.6624	36.6469
KRG16-104	1,194	137.6750	36.6484
KRG16-111	850	137.6820	36.6510
KRG16-112	850	137.6795	36.6525

References

Aitken, M.J., 1985. Thermoluminescence Dating. Academic Press, London.

Guralnik B., Jain, M., Herman, F., Paris, R.B., Harrison, T.M., Murray, A.S., Valla, P.G., Rhodes, E.J., 2013. Effective closure temperature in leaky and/or saturating thermochronometers. Earth and Planetary Science Letters. 384, 209-218.

Guralnik, B., Jain, M., Herman, F., Ankjærgaard, C., Murray, A.S., Valla, P.G., Preusser, F., King, G.E., Chen, R., Lowick, S.E., Kook, M., Rhodes, E.J., 2015a. OSL-thermochronology of feldspar from the KTB borehole, Germany. Earth and Planetary Science Letters 423, 232-243.

Guralnik, B., Li, B., Jain, M., Chen, R., Paris, R.B., Murray, A.S., Li, S.H., Pagonis, V., Valla, P.G. and Herman, F., 2015b. Radiation-induced growth and isothermal decay of infrared-stimulated luminescence from feldspar. Radiation Measurements, 81, 224-231.

Ikeya, M., 1993. *New applications of electron spin resonance: dating, dosimetry and microscopy*. World Scientific.

King, G.E., Guralnik, B., Valla, P.G. and Herman, F., 2016a. Trapped-charge thermochronometry and thermometry: A status review. *Chemical Geology*, *446*, pp.3-17.

King, G.E., Burow, C., Roberts, H.M.R. & Pearce, N.J.P., Accepted. Age determination using feldspar: evaluating fading-correction model performance. Radiation Measurements.

Lambert, R., King, G.E., Valla, P., Herman, F., In Review. Validating multiple first-order kinetic models for feldspar thermal decay in luminescence thermochronometry. Radiation Measurements.

Lambert, R., King, G.E., Valla, P., Herman, F., In Revision. Towards OSL-thermochronometry of the Mont Blanc massif: Experimental investigations into constraining feldspar thermal decay. Radiation Measurements.

Li, Y., Tsukamoto, S., Long, H., Zhang, J., Yang, L., He, Z. and Frechen, M., 2018. Testing the reliability of fading correction methods for feldspar IRSL dating: A comparison between natural and simulated-natural dose response curves. *Radiation Measurements*.

Li, B. and Li, S.H., 2011. Luminescence dating of K-feldspar from sediments: a protocol without anomalous fading correction. *Quaternary Geochronology*, *6*(5), pp.468-479.

Li, B. and Li, S.H., 2013. The effect of band-tail states on the thermal stability of the infrared stimulated luminescence from K-feldspar. *Journal of Luminescence*, *136*, pp.5-10.

Riedesel, S., King, G. E., Prasad, A. K., Kumar, R., Finch, A. A., Jain, M., In Review. Optical determination of band-tail width, depth and excited state of the IRSL trap in feldspar. Radiation Measurements.

Schmidt, C., Friedrich, J., Adamiec, G., Chruścińska, A., Fasoli, M., Kreutzer, S., Martini, M., Panzeri, L., Polymeris, G.S., Przegiętka, K. and Valla, P.G., King, G.E., Sanderson, D.C.W., 2018. How reproducible are kinetic parameter constraints of quartz luminescence? An interlaboratory comparison for the 110° C TL peak. *Radiation measurements*, *110*, pp.14-24.

Toyoda, S. and Ikeya, M., 1991. Thermal stabilities of paramagnetic defect and impurity centers in quartz: Basis for ESR dating of thermal history. *Geochemical Journal*, *25*(6), pp.437-445.